Chinese Chemical Letters 37 (2026) 112790

Contents lists available at ScienceDirect

Chinese Chemical Letters

journal homepage: www.elsevier.com/locate/cclet

Functional analysis of a diterpene synthase for jiangxidienes and jiangxienols biosynthesis from *Streptacidiphilus jiangxiensis*

Botao Yan[a,c], Hongran Chen[b], Zixin Deng[a,b], Mingguo Jiang[c,*], Min Xu[a,*], Anwei Hou[a,*]

[a] *Tianjin Institute of Industrial Biotechnology, Chinese Academy of Sciences, Tianjin 300308, China*
[b] *Haihe Laboratory of Synthetic Biology, Tianjin 300308, China*
[c] *Guangxi–Indonesia Joint Laboratory for Intelligent Exploration of Microbial Resources, Guangxi Key Laboratory of Polysaccharide Materials and Modification, School of Marine Sciences and Biotechnology, Guangxi Minzu University, Nanning 530008, China*

ARTICLE INFO

Article history:
Received 23 December 2025
Revised 15 April 2026
Accepted 16 April 2026
Available online 21 April 2026

Keywords:
Streptacidiphilus
Diterpene
Terpene synthase
Cyclisation mechanism
P450

ABSTRACT

This study identifies and characterises a previously unknown diterpene synthase, SjJS, from the acidophilic actinomycete *Streptacidiphilus jiangxiensis*. Genome mining and heterologous expression demonstrated that *S*treptacidiphilus *j*iangxiensis *J*iangxidiene *S*ynthase (SjJS) accepts both farnesyl pyrophosphate (FPP) and geranylgeranyl pyrophosphate (GGPP) as substrates to produce a diverse terpene profile, including two new diterpenes, jiangxidiene A (**1**) and B (**2**). Comprehensive ^{13}C-labelling experiments combined with computational analyses delineated its intricate cyclisation mechanism and revealed two possible pathways. Structure-guided mutagenesis enabled the accumulation of key intermediate-derived products, jiangxienols A–D (**4**, **7**, **8**, and **10**), thereby allowing a clear differentiation between the two proposed cyclisation pathways and leading to the formation of several additional diterpenes. In addition, a cytochrome P450 encoded adjacent to the *sjjs* gene was shown to oxidise jiangxidiene A (**1**), the major diterpene product, yielding jiangxienoide B (**12**) and jiangxienol E (**13**). Further cytotoxicity assays were performed for the isolated compounds, among which jiangxidiene A (**1**) gave the lowest half maximal inhibitory concentration (IC_{50}) values (15–20 μg/mL) against the tested human cancer cell lines.

© 2026 Published by Elsevier B.V. on behalf of Chinese Chemical Society and Institute of Materia Medica, Chinese Academy of Medical Sciences.

Terpenoids represent one of the most structurally diverse and functionally versatile families of natural products (NPs), with over 100,000 structures reported to date. They are widely distributed among plants, microorganisms, and marine organisms, exhibiting remarkable pharmacological activities and significant industrial relevance [1–4]. Typical examples include the anticancer drug taxol [5], the antimalarial compound artemisinin [6], the cooling and fragrance agent menthol [7], and the biopolymer material natural rubber [8], which in together highlight the broad medical, cosmetic, and material applications of this vast group of NPs. Among them, diterpenes, characterised by their complex polycyclic skeletons and diverse bioactivities, have long attracted significant attention in NP chemistry and synthetic biology [9–15].

However, compared to their abundant counterparts of plant-derived diterpenes [1,2,10–12,16], the biosynthetic potential of microbial, particularly for those actinomycete-derived diterpenes, remains insufficiently explored. Although strains from the genus of *Streptomyces* have been extensively studied and has yielded a wide variety of terpenoid metabolites [1,9,17–20], its close acidophilic relative *Streptacidiphilus* has been rarely investigated in this context. Notably, recent genomic analyses have revealed that *Streptacidiphilus* harbors abundant terpene synthase genes [21], suggesting that this genus may represent an untapped reservoir of structurally diverse terpenoids.

In this study, we identified a previously uncharacterised diterpene synthase from *Streptacidiphilus jiangxiensis* through genome mining. *In vitro* assays and heterologous expression confirmed that this enzyme catalyses the formation of new diterpenes. In addition, isotopic labelling experiments, together with density functional theory (DFT) calculations and mutagenesis studies, elucidated the cyclisation mechanism of this enzyme. Furthermore, the function of the adjacent cytochrome P450 was characterised, and the antitumor activities of several major isolates were evaluated against four human cancer cell lines. This work broadens our understanding of the terpenoid metabolic capacity of *Streptacidiphilus* and provides new insights into the functional diversity of bacterial diterpene synthases.

The genome of *Streptacidiphilus jiangxiensis* NBRC 100920 was searched using HMMER (http://hmmer.org/) [22]. with the HMM seed profile (PF19086) for class I terpene synthases (TSs), lead-

* Corresponding authors.
E-mail addresses: mzxyjiang@163.com (M. Jiang), xumin@tib.cas.cn (M. Xu), anwei.hou@tib.cas.cn (A. Hou).

https://doi.org/10.1016/j.cclet.2026.112790
1001-8417/© 2026 Published by Elsevier B.V. on behalf of Chinese Chemical Society and Institute of Materia Medica, Chinese Academy of Medical Sciences.

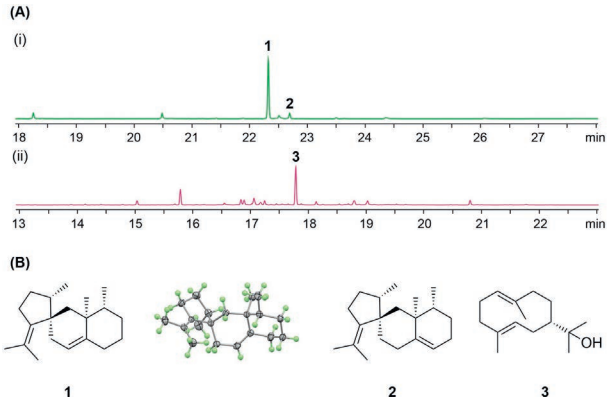


Fig. 1. Products of SjJS. (A) Total ion chromatograms (TICs) of SjJS incubated with GGPP (i) and FPP (ii), analyzed by gas chromatography-mass spectrometry (GC–MS). (B) Chemical structures of products **1**–**3**. The absolute configuration of **1** was determined by X-ray crystallography (CDCC 2516818).

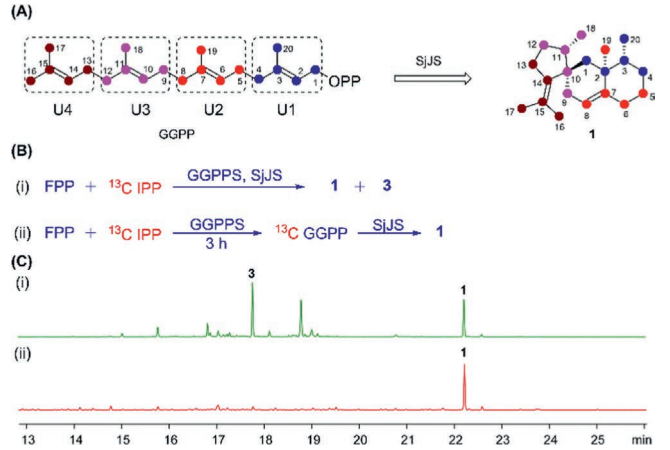


Fig. 2. ^{13}C-labelling strategy for the preparation of labelled GGPP and **1**. (A) Schematic representation of the four isoprene units constituting GGPP and the corresponding labelling pattern in **1**. (B) Two reaction setups (i and ii) for the synthesis of ^{13}C-labelled GGPP and corresponding ^{13}C-labelled **1** using FPP and ^{13}C-labelled IPP in the presence of GGPPS and SjJS. (i) All substrates and enzymes were mixed simultaneously and incubated overnight. (ii) Substrate and GGPPS were first incubated for 3 h, after which SjJS was added. (C) TICs of the two reactions described in (B).

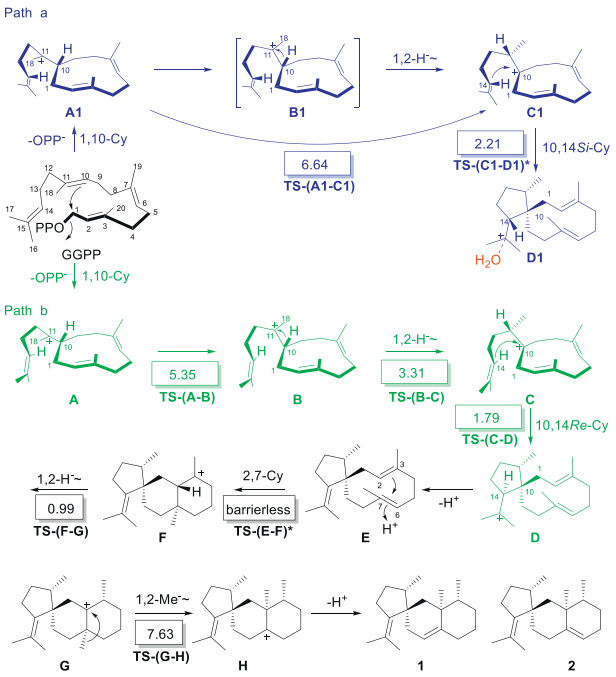
ing to the identification of six putative TSs (TS-01–TS-06, Table S1 in Supporting information). Phylogenetic analysis including over 90 characterised TSs (Fig. S1 in Supporting information) [23]. showed that TS-01 is homologous to geosmin synthase [24]. and contains two typical catalytic domains. Similarly, TS-02 clusters with sesquiterpene synthases such as germacrene D-4-ol synthase (45% identity) [25]. and cubebene synthase (47% identity) [26]. In addition, TS-03 shares 55% sequence identity with selina-4(15),7(11)-diene synthase [27], suggesting a high degree of functional similarity. TS-05 clusters with 2-methylisoborneol synthase [28], a terpene synthase whose function appears to be relatively conserved. Taken together, these phylogenetic relationships suggest that the functions of these four TSs may be provisionally inferred based on phylogenetic clustering. In contrast, TS-04 and TS-06 cluster with two diterpene synthases (venezuelaene synthase [29]. and AriT [30]) with <30% sequence identity, indicating that they may represent novel diterpene synthases.

The two TS genes were then synthesised after codon optimisation for expression in *Escherichia coli* and subsequently cloned into pET-28a(+) vector for heterologous protein expression. TS-04 expressed well in soluble form; however, TS-06 was largely insoluble (Fig. S2 in Supporting information). Enzymatic assays of TS-04 were then performed using geranyl pyrophosphate (GPP), farnesyl pyrophosphate (FPP), geranylgeranyl pyrophosphate (GGPP), and geranylfarnesyl pyrophosphate (GFPP) as substrates. The results showed that TS-04 could utilize FPP and GGPP as substrates, indicating that it possesses both sesquiterpene and diterpene synthase activities (Fig. 1 and Fig. S3 in Supporting information). The major products were further obtained by co-expressing TS-04 with the corresponding FPP or GGPP synthase genes in an engineered *E. coli* chassis [31]. Based on detailed nuclear magnetic resonance (NMR) analysis, the diterpene products **1** (Table S3 and Figs. S4–S11 in Supporting information) and **2** (Table S4 and Figs. S12–S19 in Supporting information) were identified as two new compounds featuring a carbon skeleton the same as that of SpcB, which is the enantiomer of compound **1** and has only been reported in a patent [32]. As the producing strain and biosynthetic enzyme responsible for SpcB formation were not disclosed in the patent, we therefore designated the two new compounds as jiangxidiene A and jiangxidiene B, respectively, to reflect their biological origin. The main sesquiterpene product **3** was identified as hedycaryol by comparison of its MS (Fig. S3 in Supporting information) and ^{1}H NMR spectra (Fig. S20 in Supporting information) with those reported in the literature [33]. Accordingly, the enzyme TS-04 was designated as *Streptacidiphilus jiangxiensis* Jiangxidiene Synthase (SjJS).

The cyclisation process of GGPP leading to the formation of jiangxidienes remains unclear. However, isotopic labelling represents a powerful strategy to elucidate the underlying cyclisation mechanism of TS [18,34,35]. Since position-specific labelled isopentenyl pyrophosphates (IPPs) at five defined sites have already been synthesised and are available [36], it should be feasible to label all 20 carbon positions of GGPP through the combined use of prenyltransferase and isopentenyl diphosphate isomerase (IDI) [37]. Principally, by combining FPP with ^{13}C-labelled IPPs, the first C_5 unit of GGPP can be labelled, yielding (U1–^{13}C)GGPP (Fig. 2A and Fig. S21 in Supporting information), which comprises five position-specific isotopomers, (1–^{13}C), (2–^{13}C), (3–^{13}C), (4–^{13}C), and (20–^{13}C)GGPP. Similarly, coupling GPP or DMAPP with ^{13}C-labelled IPPs and unlabelled IPP affords (U2–^{13}C)GGPP and (U3–^{13}C)GGPP, respectively. Furthermore, through IDI-mediated isomerisation of ^{13}C-labelled IPPs followed by condensation with unlabelled IPP, (U4–^{13}C)GGPP can be obtained.

Then, detailed enzymatic assays were performed by incubating GGPP synthase (GGPPS) [31], SjJS, FPP, and (1–^{13}C)IPP together. Under these conditions, both the diterpene **1** and the sesquiterpene **3** were produced (Figs. 2B(i) and 2C(i)), as SjJS exhibits sesquiterpene synthase activity and can directly convert FPP into **3**. To optimize the reaction, FPP, (1–^{13}C)IPP, and GGPPS were first incubated to allow GGPPS to elongate FPP into (1–^{13}C)GGPP. After this elongation step, SjJS was subsequently added to catalyse the cyclisation. Using this sequential process, the major product obtained was the diterpene **1** (Figs. 2B(ii) and 2C(ii)). Following the same strategy, (2–5–^{13}C)IPPs were also converted into the corresponding GGPPs. Likewise, GPP and DMAPP were elongated with ^{13}C-labelled IPPs by FPP synthase (FPPS) and GPP synthase (GPPS) [31], respectively, and then further elongated with GGPPS and unlabelled IPP to afford (U2–^{13}C)GGPP and (U3–^{13}C)GGPP. For ^{13}C-labelled DMAPPs, they were generated by the isomerisation of ^{13}C-labelled IPPs catalysed by IDI within 1 h, and subsequently elongated by GPPS and GGPPS to afford (U4–^{13}C)GGPP (Fig. S22 in Supporting information). All of these labelled GGPPs were individually converted by SjJS to yield a set of ^{13}C-labelled isotopomers of compound **1**, collectively covering all twenty carbon positions (Fig. 2A and Fig. S23 in Supporting information).

The labelling results clearly demonstrate how GGPP folds within the active site of SjJS, revealing that a Me-19 migration occurs dur-



Scheme 1. Proposed cyclisation mechanism of SjJS from GGPP to **1** and **2**. Key carbocation intermediates are shown. Boxed numbers indicate transition state energy barriers (kcal/mol, mPW1PW91/6–311+G(d,p)//B3LYP/6–31G(d,p)). Barriers for **TS-(C1–D1)*** and **TS-(E–F)*** are referenced to intermediates **C1** and **E** using water- and NH_3-assisted models, respectively.

ing the cyclisation cascade. Based on these findings, a plausible enzyme-catalysed mechanism is proposed (Scheme 1). GGPP first adopts a conformation that enables the initial 1,10-cyclisation to generate cation **A**. The Me-18 group must then rotate into a perpendicular orientation relative to H-10 (intermediate **B**), thereby facilitating a subsequent 1,2-hydride migration to form intermediate **C**. Intermediate **C** then undergoes a 10,14-cyclisation, during which attack of C14 onto C10 can occur from either the *Si* or *Re* face of the double bond. These two approaches generate distinct downstream carbocation intermediates, designated **D1** (path a) and **D** (path b), respectively. To clearly distinguish the conformations adopted by intermediates **A**–**C** in the two mechanistic pathways, the corresponding intermediates in path a are denoted as **A1**–**C1**, respectively. Subsequent deprotonation from either pathway yields the same intermediate **E**. Protonation of **E** then initiates a further cyclisation to form intermediate **F**, which undergoes a 1,2-hydride shift followed by a Me-19 migration to give cation **H**. Finally, deprotonation of **H** furnishes the observed products **1** and **2**.

To distinguish between the two possible pathways, DFT calculations were performed [38]. The potential energy profile for path b was calculated (Fig. S24 and Table S5 in Supporting information). Starting from cation **A**, rotation of the Me-18 proceeds over a barrier of 5.35 kcal/mol, forming intermediate **B**. The subsequent 1,2-hydride shift occurs through a low-lying transition state ($\Delta G^{\ddagger} = 3.31$ kcal/mol) to afford intermediate **C**. From **C**, formation of **D** involves crossing another small barrier of 1.79 kcal/mol. Following this, deprotonation affords intermediate **E**, and subsequent protonation-induced 2,7-cyclisation proceeds in a barrierless fashion, generating **F** and accompanied by a pronounced energy drop of −17.17 kcal/mol, indicating a highly exergonic step. From **F**, a 1,2-hydride shift occurs almost barrierlessly ($\Delta G^{\ddagger} = 0.99$ kcal/mol) to produce **G**, followed by migration of Me-19 to form **H** ($\Delta G^{\ddagger} = 7.63$ kcal/mol). The relatively low activation barriers indicate that these rearrangements along path b are energetically facile within the enzyme's active site.

For path a, DFT calculations were performed on the first four intermediates (Fig. S25 and Table S6 in Supporting information), as the remaining steps are identical to those in path b. The calculations show that intermediate **B1** is not a stable minimum, and **A1** directly converts to **C1** by overcoming a modest barrier ($\Delta G^{\ddagger} = 6.64$ kcal/mol). Furthermore, **C1** cannot cyclise to a stable **D1** intermediate in the absence of assistance. In contrast, when a water molecule is included to stabilize the developing cationic center, the cyclisation to **D1** proceeds smoothly with a low barrier of 2.21 kcal/mol. Based on the calculations, both pathways are feasible. However, path a requires assistance from a water molecule for the formation of intermediate **D1**, and **B1** does not exist as a stable species. Since **D1** differs structurally from **D**, obtaining products that retain the configuration of H-14, for example, from enzyme variants bearing subtle active-site modifications, could provide direct experimental evidence to distinguish which pathway is actually operative.

Thereafter, the three-dimensional structure of SjJS was generated by AlphaFold 3 [39], and GGPP was subsequently docked into the modeled active site using AutoDock [40]. Residues constituting the GGPP-binding pocket are highlighted in stick representation (Fig. 3A). Further molecular dynamics (MD) analysis of intermediates **D1** revealed that residue E96 plays a key role in the 2,7-cyclisation step by serving as a proton donor (Figs. S26 and S27 in Supporting information). In addition, the deprotonated carboxylate form of E96 may also function as a general base to facilitate deprotonation of intermediate **H** (Figs. S28 and S29 in Supporting information). Therefore, E96 was not subjected to mutagenesis. Instead, several residues located in the lower region of the active-site pocket were selected for site-directed mutagenesis, as modifications at these positions were anticipated to have minimal impact on the initial cyclisation step. The enzyme variants Y76F, M202L, M202S, V205I, T238V, V322A, and V322T were then constructed, and their product profiles were analysed (Fig. S30 in

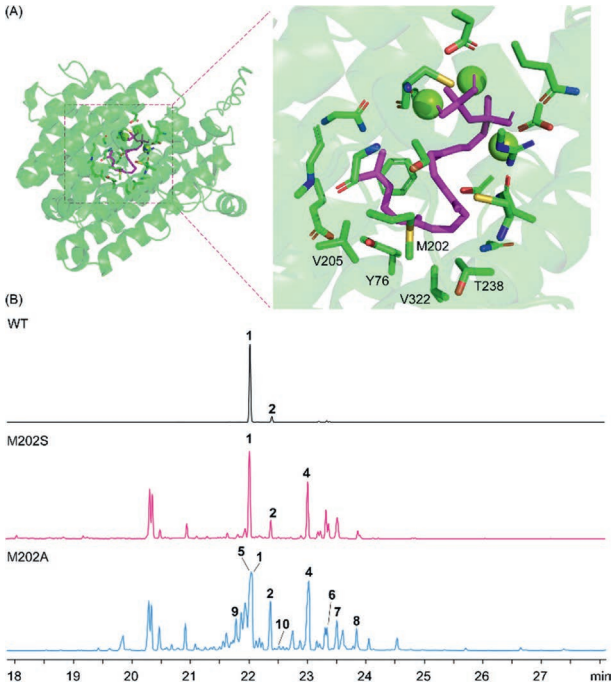


Fig. 3. Mutational analysis of SjJS. (A) Structural model of SjJS predicted by AlphaFold 3, with key residues shaping the active-site pocket shown in stick representation and the docked GGPP substrate rendered in purple. The trinuclear Mg^{2+} cluster is depicted as green spheres. (B) TICs of the *in vitro* enzymatic products of the WT enzyme and the M202S variant, and the *in vivo* products produced by the M202A variant heterologously expressed in an *E. coli* chassis.

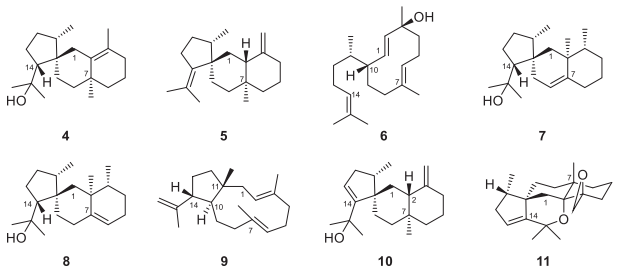


Fig. 4. Isolated products from the SjJS M202A variant.

Supporting information). The Y76F and M202L mutants displayed product profiles nearly identical to that of the wild-type (WT) enzyme. In contrast, the V205I, T238V, V322A, and V322T variants produced higher amounts of **2**, likely due to reduced steric hindrance at these positions, which permits intermediate **H** to move more freely within the active site. Notably, the M202S mutant generated several new products, with one major product shifted to a new compound **4**. To further probe the role of this residue, we performed saturation mutagenesis at position 202 and found that the M202A variant produced more products (Fig. 3B and Fig. S31 in Supporting information). Subsequent purification and NMR analysis led to the identification of 8 additional products **4**–**11** (Fig. 4, Figs. S32–S109 and Tables S7–S24 in Supporting information).

To exclude the possibility of misassigning the relative configurations, DP4+ [41]. analyses were performed for compounds **4** and **8** using two diastereomeric models in which H-14 was oriented either upward or downward (Figs. S41 and S76 in Supporting information). In both cases, the results indicated that H-14 in both **4** and **8** is oriented upward, and that both compounds incorporate a hydroxyl group at C-15, consistent with the proposed path a. Moreover, MD simulations indicate that a water molecule can stably reside near C-15 in the SjJS–**D1** complex (Figs. S26 and S27 in Supporting information). The formation of **4** and **8** can be clearly rationalised by the mechanistic pathway involving **D1** and **F1**, providing additional support that path a represents the operative cyclisation route of SjJS (Fig. S110 in Supporting information). Compounds **5**, **7**, and **10** share closely related skeletal frameworks. Compound **5** is proposed to originate from intermediate **F**, whereas the formation of **7** follows a pathway analogous to that leading to **8**. The formation of **10** might arise from non-enzymatic oxidation of compound **5** (Fig. S110). The relative configuration of **6** was also confirmed by NMR calculations and DP4+ analysis (Figs. S58 and S59 in Supporting information), and its formation can be rationalised by a C-1–αH migration toward the cationic centre at C-10, followed by nucleophilic attack by water, ultimately yielding **6** (3–*epi*-obscuronatin [13], Fig. S110). Based on this mechanism, its absolute configuration can be tentatively assigned as 3*S*,10*R*,11*S*.

Compound **11** was not detected in the *in vivo* assays but was obtained after purification using $AgNO_3$-coated thin-layer chromatography (TLC) plates. Its structure was further verified by NMR calculations, and the calculated ^{13}C NMR chemical shifts showed a linear correlation of over 0.99 with the experimental data, confirming the structural assignment (Fig. S109). Its formation might occur *via* an unknown oxidation process during purification. The formation of compound **9** deviates from the main cyclisation pathway and may arise from an alternative initial 1,11–10,14 cyclisation sequence facilitated by a conformational change of the terminal isoprene unit of GGPP (Fig. S110). Similar cyclisation mechanisms have been reported for several terpene synthases [1,42]. However, its specific rotation differs from that of the previously described (1*S*,3*E*,7*E*,11*R*,12*S*)-dolabella-3,7,18-triene, indicating that **9** is its enantiomer. In addition, compounds **4**, **7**, **8**, and **10** were designated as jiangxienol A, B, C, and D, respectively;

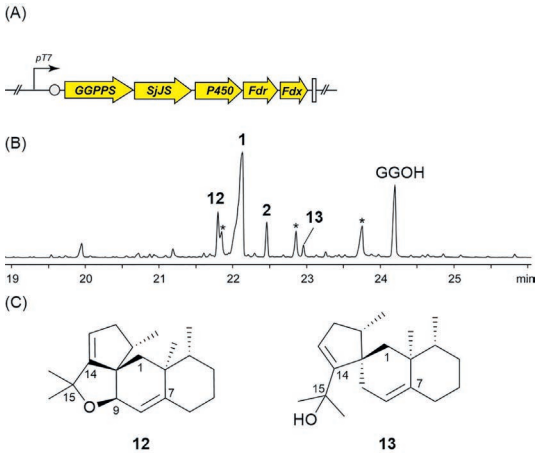


Fig. 5. Functional analysis of the P450 enzyme associated with SjJS. (A) Schematic diagram of the engineered expression cassette under the control of T7 promoter. The cassette contains GGPPS, SjJS, the P450 enzyme, and its redox partners *Sel*FdR0978 (Fdr) and *Sel*Fdx1499 (Fdx). A ribosome binding site (circle) is placed downstream of the promoter, and a transcription terminator is depicted as a narrow rectangular block at the end of the cassette. (B) TIC of the metabolites produced by the recombinant *E. coli* chassis expressing this cassette. Asterisks indicate endogenous metabolites from the host strain; GGOH denotes geranylgeraniol. (C) Chemical structures of the oxidation products **12** and **13**.

compound **5** was designated as jiangxidiene C, and compound **11** was designated as jiangxienoide A.

A cytochrome P450 gene (WP_042443903), located adjacent to the *sjjs* gene, was identified in the genome and subsequently codon-optimized for heterologous expression in *E. coli*. The gene encoding this P450 was cloned into pET-28a(+), and the recombinant protein was successfully expressed in a soluble form in *E. coli* (Fig. S2). To investigate its function, the P450 together with a broadly applicable redox partner pair (*Sel*Fdx1499/*Sel*FdR0978) [43], GGPPS, and SjJS were co-expressed under the control of T7 promoter in the *E. coli* chassis (Fig. 5A). After a 5-day fermentation, two oxidised products were detected from the culture extract (Fig. 5B and Fig. S111 in Supporting information). Following comprehensive purification, compounds **12** (Table S25 and Figs. S112–S119 in Supporting information) and **13** (Table S26 and Figs. S120–S127 in Supporting information) were isolated and structurally characterised as oxidised products derived from **1** (Fig. 5C), and they were designated as jiangxienoide B and jiangxienol E, respectively.

In vitro cytotoxicity assays against four human cancer cell lines, HeLa (cervical carcinoma), KYSE-150 (esophageal squamous cell carcinoma), NCI-H1975 (non-small cell lung cancer), and SGC7901 (gastric carcinoma), as well as the normal human lung fibroblast cell line MRC-5 revealed only modest or negligible activity for the major isolated compounds (Table S27 in Supporting information). Compound **1** gave the lowest half maximal inhibitory concentration (IC_{50}) values, among the tested compounds, ranging from 15 μg/mL to 20 μg/mL against the cancer cell lines (20.19 μg/mL *vs.* HeLa, 19.70 μg/mL *vs.* both KYSE-150 and NCI-H1975, and 15.65 μg/mL *vs.* SGC7901) and 18.14 μg/mL against MRC-5. Compound **6** showed measurable responses only toward SGC7901 (IC_{50} = 18.91 μg/mL), while IC_{50} values above 25 μg/mL were obtained for the other tested cancer cell lines. By contrast, compounds **2**, **4**, **5**, **8**, **9**, **12**, and **13** yielded IC_{50} values above 25 μg/mL across all tested cancer cell lines. Cytotoxicity toward the normal human fibroblast cell line MRC-5 was not further evaluated for these compounds.

Overall, this study establishes *Streptacidiphilus* as a previously underexplored yet productive source of structurally unusual diterpenoid NPs. By integrating genome mining, heterologous expres-

sion, and *in vitro* enzymatic assays, we identified and functionally characterised a novel diterpene synthase, SjJS, capable of generating new diterpenoids. The application of position-specific ^{13}C isotopic labelling, in combination with DFT calculations and site-directed mutagenesis, provided detailed mechanistic insights into the complex cyclisation process and revealed a key residue governing product formation. Furthermore, functional characterisation of a cytochrome P450 encoded adjacent to *sjjs* uncovered an additional oxidative tailoring step that further diversifies the products. Bioactivity evaluation showed that jiangxidiene A yielded IC_{50} values in the range of 15–20 μg/mL against four human cancer cell lines. Collectively, this work expands our understanding of diterpenoid biosynthesis, highlights the catalytic versatility of bacterial terpene synthases, and underscores the potential of *Streptacidiphilus* spp. as a valuable reservoir for the discovery of novel terpenoids and biocatalysts.

Declaration of generative AI and AI-assisted technologies in the writing process

During the preparation of this manuscript, the authors used ChatGPT (OpenAI, GPT-5, 2025 version) to assist with language editing and improvement of clarity. The authors subsequently reviewed and revised the content and take full responsibility for the final version of the manuscript.

CRediT authorship contribution statement

Botao Yan: Writing – original draft, Investigation. **Hongran Chen:** Investigation. **Zixin Deng:** Supervision. **Mingguo Jiang:** Writing – review & editing, Supervision. **Min Xu:** Writing – review & editing, Supervision. **Anwei Hou:** Writing – review & editing, Writing – original draft, Project administration, Supervision, Conceptualization.

Declaration of competing interest

The authors declare that they have no known competing financial interests or personal relationships that could have appeared to influence the work reported in this paper.

Acknowledgments

This work was financially supported by National Key Research and Development Program of China (No. 2023YFA0916200), the Innovation Fund and Major Project of the Haihe Laboratory of Synthetic Biology (Nos. 22HHSWSS00007 and 22HHSWSS00001), the Tianjin Synthetic Biotechnology Innovation Capacity Improvement Project (No. TSBICIP-CXRC-065), as well as National Natural Science Foundation of China (Nos. 22107038 and 32460009) and Science and Technology Major Project of Guangxi (No. AA18242026). We acknowledge the Biodesign Center of the Tianjin Institute of Industrial Biotechnology, Chinese Academy of Sciences, for computational support, as well as Dr. Jie Zhang and the Structural Biology Platform for assistance with single-crystal X-ray diffraction analysis of small molecules. We also thank Dr. Yi Cai from the Systems Biology Center for NMR analytical services.

Supplementary materials

Supplementary material associated with this article can be found, in the online version, at doi:10.1016/j.cclet.2026.112790.

References

[1] X. Wei, W. Ning, C.A. McCadden, et al., Nat. Commun. 16 (2025) 3721–3729.
[2] T. Zeng, Y. Chen, Y. Jian, et al., New. Phytol. 235 (2022) 662–673.
[3] J.D. Rudolf, T.A. Alsup, B. Xu, et al., Nat. Prod. Rep. 38 (2021) 905–980.
[4] A. Ludwiczuk, K. Skalicka-Woźniak, M.I. Georgiev, Terpenoids, in: S. Badal, R. Delgoda (Eds.), Pharmacognosy, Academic Press, Boston, 2017, pp. 233–266.
[5] E.K. Rowinsky, R.C. Donehower, N. Engl. J. Med. 332 (1995) 1004–1014.
[6] Y. Tu, Nat. Med. 17 (2011) 1217–1220.
[7] R. Eccles, J. Pharm. Pharmacol. 46 (1994) 618–630.
[8] H. Mooibroek, K. Cornish, Appl. Microbiol. Biotechnol. 53 (2000) 355–365.
[9] J.S. Dickschat, Angew. Chem. Int. Ed. 58 (2019) 15964–15976.
[10] P. Zerbe, B. Hamberger, M.M.S. Yuen, et al., Plant Physiol. 162 (2013) 1073–1091.
[11] R.J. Peters, Nat. Prod. Rep. 27 (2010) 1521–1530.
[12] E. Baloglu, D.G.I. Kingston, J. Nat. Prod. 62 (1999) 1448–1472.
[13] G.B. Tabekoueng, B. Goldfuss, J.S. Dickschat, Org. Lett. 27 (2025) 10821–10824.
[14] G.B. Tabekoueng, H. Li, K. Yang, et al., Angew. Chem. Int. Ed. 64 (2025) e202513149.
[15] X. Wei, W. DeSnoo, Z. Li, et al., J. Am. Chem. Soc. 147 (2025) 16293–16300.
[16] A.P. Wardana, N.S. Aminah, M. Rosyda, et al., Heliyon. 7 (2021) e07777.
[17] J.D. Rudolf, L.B. Dong, H. Cao, et al., J. Am. Chem. Soc. 138 (2016) 10905–10915.
[18] P. Rabe, J. Rinkel, E. Dolja, et al., Angew. Chem. Int. Ed. 56 (2017) 2776–2779.
[19] J. Rinkel, S.T. Steiner, J.S. Dickschat, Angew. Chem. Int. Ed. 58 (2019) 9230–9233.
[20] M.J. Smanski, Z. Yu, J. Casper, et al., Proc. Natl. Acad. Sci. U. S. A. 108 (2011) 13498–13503.
[21] A. Malik, Y.R. Kim, S.B. Kim, Genes 11 (2020) 1166.
[22] R.D. Finn, J. Clements, S.R. Eddy, Nucleic. Acids. Res. 39 (2011) W29–W37.
[23] Y. Li, X. Xiang, Z. Ren, et al., Microorganisms 13 (2025) 1479.
[24] J. Jiang, X. He, D.E. Cane, Nat. Chem. Biol. 3 (2007) 711–715.
[25] I. Burkhardt, N.B. Kreuzenbeck, C. Beemelmanns, et al., Org. Biomol. Chem. 17 (2019) 3348–3355.
[26] Y. Yamada, T. Kuzuyama, M. Komatsu, et al., Proc. Natl. Acad. Sci. U. S. A. 112 (2015) 857–862.
[27] P. Baer, P. Rabe, K. Fischer, et al., Angew. Chem. Int. Ed. 53 (2014) 7652–7656.
[28] C.M. Wang, D.E. Cane, J. Am. Chem. Soc. 130 (2008) 8908–8909.
[29] Z. Li, Y. Jiang, X. Zhang, et al., ACS Catal. 10 (2020) 5846–5851.
[30] Y.L. Hu, Q. Zhang, S.H. Liu, et al., Chem. Sci. 14 (2023) 3661–3667.
[31] G. Bian, Y. Han, A. Hou, et al., Metab. Eng. 42 (2017) 1–8.
[32] H. Ge, S. Liu, Y. Hu, et al., Patent, CN117756597A, 2024.
[33] H. Xu, N.D. Lackus, T.G. Köllner, et al., Org. Lett. 24 (2022) 587–591.
[34] A. Hou, J.S. Dickschat, Angew. Chem. Int. Ed. 59 (2020) 19961–19965.
[35] A. Hou, B. Goldfuss, J.S. Dickschat, Angew. Chem. Int. Ed. 60 (2021) 20781–20785.
[36] R. Liu, Z. Ren, Z. Deng, et al., Tetrahedron. 168 (2024) 134356.
[37] F. Zhu, X. Zhong, M. Hu, et al., Biotechnol. Bioeng. 111 (2014) 1396–1405.
[38] D.J. Tantillo, Nat. Prod. Rep. 28 (2011) 1035–1053.
[39] J. Abramson, J. Adler, J. Dunger, et al., Nature 630 (2024) 493–500.
[40] G.M. Morris, R. Huey, W. Lindstrom, et al., J. Comput. Chem. 30 (2009) 2785–2791.
[41] N. Grimblat, M.M. Zanardi, A.M. Sarotti, J. Org. Chem. 80 (2015) 12526–12534.
[42] J. Rinkel, L. Lauterbach, J.S. Dickschat, Angew. Chem. Int. Ed. 58 (2019) 452–455.
[43] X. Liu, F. Li, T. Sun, et al., Commun. Biol. 5 (2022) 791.